Trace, Verify, and Correct: A Training-Free Framework for Spatial Reasoning in Multimodal LLMs

Yang Yang[1*], Jiawei Chen[1,2*], Tairan Chen[3], Zhaoxia Yin[1†]

[1]Shanghai Key Laboratory of Multidimensional Information Processing, East China Normal University
[2]Zhongguancun Academy
[3]Stevens Institute of Technology

arXiv:2608.04759v1 [cs.CV] 5 Aug 2026

Abstract

Although Multimodal Large Language Models (MLLMs) have made substantial progress, their spatial reasoning may still produce intermediate judgments inconsistent with the input image, allowing errors to propagate through the reasoning chain and affect the final answer. Existing methods mainly improve spatial reasoning through training or additional spatial information, without considering whether the reasoning process itself is faithful to the model input. Our study shows that unfaithful reasoning chains significantly reduce final-answer accuracy. To address this issue, we propose a modular and training-free framework for spatial reasoning verification and correction. The framework constructs a Spatial Evidence Graph (SEG), which associates atomic spatial evidence extracted from Chain-of-Thought reasoning with visual entities, spatial relations, source steps, and visual evidence. Spatial Evidence Reliability Assessment (SERA) evaluates the reliability of visual evidence based on object existence, localization, and geometric measurements. The framework then identifies the earliest spatial evidence unit contradicted by reliable visual evidence and guides the original MLLM to revise the subsequent reasoning and final answer. Across 15 model–dataset settings, our method achieves an average accuracy of 68.94%, outperforming the compared baselines by 8.55 percentage points on average. Our code will be open-sourced.

1 Introduction

MLLMs have recently achieved substantial progress in visual question answering (Kuang et al., 2025; Zhong et al., 2026), image understanding (Jiang et al., 2026; Meng et al., 2025), and cross-modal reasoning (Ma et al., 2026; Jiang et al., 2025). Nevertheless, spatial reasoning remains a major challenge. To solve complex spatial problems, MLLMs commonly employ Chain-of-Thought (CoT) reasoning to decompose the problem into a sequence of intermediate steps before deriving the final answer. However, an intermediate spatial judgment that is inconsistent with the visual input may be reused as a premise in subsequent steps, allowing local errors to propagate through the reasoning chain and affect the final answer. Reliable spatial reasoning is therefore essential for extending multimodal models from static image understanding to interaction with real-world environments (Chen et al., 2026a; Ding et al., 2025; Liu et al., 2024b). For example, in high-stakes domains such as autonomous driving and robotics, incorrect spatial judgments may lead to erroneous decisions, resulting in substantial economic losses or even threats to human safety.

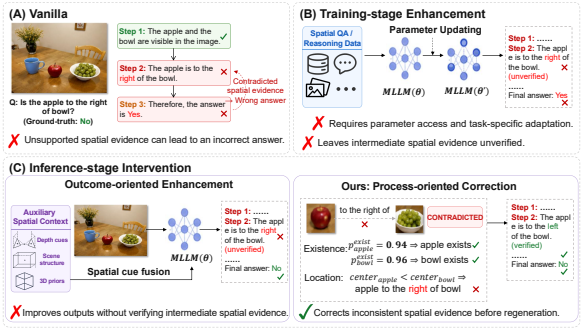

Figure 1: Motivation for perceptually faithful spatial reasoning. (A) Vanilla reasoning propagates unsupported evidence to an incorrect answer. (B) Training-stage methods require parameter access and task-specific adaptation. (C) Inference-stage methods improve outputs but leave intermediate spatial evidence unverified. Our process-oriented method verifies and corrects inconsistent spatial evidence before regeneration.

As shown in Fig. 1, prior work (Gholami et al., 2025; Wang et al., 2025b; Daxberger et al., 2025; Zhang et al., 2026; Li et al., 2026b) enhances MLLM spatial reasoning using spatial QA or reasoning data during training, but requires parameter access and adaptation to new models or tasks. To

[*]Equal contribution.
[†]Corresponding author.

avoid retraining, subsequent work (Ma et al., 2024; Roy et al., 2025; Zhu et al., 2026; Li et al., 2025b; Hua et al., 2026) introduces depth cues, structured scene representations, or 3D priors at inference time. However, these methods remain primarily outcome-oriented: they enhance the input or overall generation process without explicitly locating, verifying, or correcting intermediate spatial evidence. Consequently, intermediate reasoning errors may remain undetected and propagate to the final answer. We term consistency between intermediate spatial evidence and visual input *perceptual faithfulness* (Lv et al., 2026; Li et al., 2026a). Section 2.1 shows that perceptually unfaithful reasoning chains have significantly lower answer accuracy. We therefore adopt a process-oriented strategy that verifies and corrects spatial evidence after initial CoT generation and regenerates the affected reasoning and final answer.

Reliably correcting such unfaithful reasoning presents two key challenges. First, spatial evidence units are difficult to extract and trace. In free-form CoT, spatial judgments may be expressed implicitly and distributed across interdependent reasoning steps, making it difficult to accurately identify each evidence unit and trace it to its source step. Second, verification evidence is not always reliable. Object existence, localization, and geometric measurements may be affected by occlusion and perception errors, and correcting the CoT based on uncertain evidence may alter otherwise valid spatial judgments and degrade answer accuracy.

To meet these challenges, we propose a verification-and-correction framework for perceptually faithful spatial reasoning in MLLMs. SEG addresses evidence extraction and provenance tracing by representing each atomic CoT spatial judgment as an evidence unit while preserving its visual entities, spatial relations, and source step. SERA addresses unreliable verification evidence by assessing object existence, localization confidence, and geometric measurement quality. Based on these reliability-aware results, the framework identifies the earliest evidence unit contradicted by reliable visual evidence and guides the original MLLM to regenerate the affected reasoning and final answer. Correcting from the earliest reliably detected error improves perceptual faithfulness and final-answer accuracy while preserving valid reasoning. Our key contributions are:

- We propose a systematic verification and correction framework for spatial reasoning in MLLMs, enabling evidence-level spatial-relation verification, error localization, and reasoning revision.
- We develop the SEG and SERA to support structured provenance tracing of spatial evidence units and hierarchical reliability assessment of verification evidence.
- Our training-free and model-agnostic framework consistently improves multiple MLLMs across spatial reasoning benchmarks, achieving an average accuracy of 68.94% and outperforming the compared baselines by 8.55 percentage points on average.

Dataset	CoT Faithfulness	Acc. (%)	OR	p-value
RealWorldQA	Fully Faithful	51.10	1.99	< 0.001
	Unfaithful	34.41		

Table 1: Final-answer accuracy conditioned on CoT faithfulness for InternVL3.5-8B.

2 Why Reasoning-Level Spatial Correction Is Necessary

We investigate the necessity of reasoning-level spatial correction through three empirical analyses.

2.1 Perceptually Unfaithful Reasoning Is Associated with Lower Answer Accuracy

To examine the relationship between reasoning faithfulness and answer performance, we inspect CoTs generated by InternVL3.5-8B on RealWorldQA and annotate spatial evidence units as supported, contradicted, or inconclusive. We compare faithful CoTs, in which all evidence units are supported by the image, with unfaithful CoTs containing at least one contradicted evidence unit. As shown in Tab. 1, the two groups achieve final-answer accuracies of 51.10% and 34.41%, respectively, a difference of 16.69%. This difference is statistically significant (Fisher's exact test, OR $= 1.99$, $p < 0.001$), indicating that perceptually unfaithful spatial reasoning is significantly associated with lower final-answer accuracy. Therefore, we investigate whether improving spatial reasoning faithfulness can enhance final-answer accuracy.

2.2 Spatial Unfaithfulness Accumulates Along the Reasoning Chain

We further normalize the position of each spatial evidence unit according to its source step and define

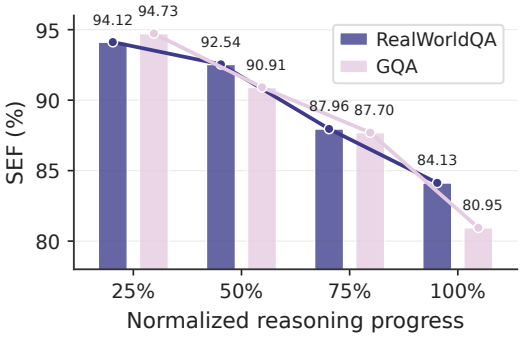

Figure 2: Cumulative spatial evidence faithfulness of Vanilla on fixed 500-sample subsets of RealWorldQA and GQA using InternVL3.5-8B.

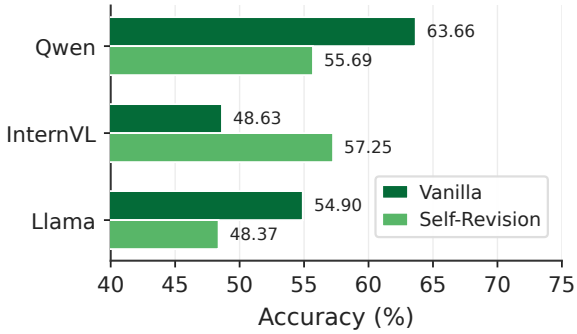

Figure 3: Effect of generic Self-Revision on the final-answer accuracy of three MLLMs on RealWorldQA.

Spatial Evidence Faithfulness at $p\%$ (SEF@p) as the cumulative faithfulness of evidence units originating within the first $p\%$ of the reasoning chain. As shown in Fig. 2, the SEF@p of Vanilla consistently decreases as reasoning progresses on both RealWorldQA and GQA, indicating that unfaithful spatial evidence can arise at different stages and gradually accumulate. Therefore, improving final-answer accuracy requires locating spatial evidence units within the reasoning chain.

2.3 Untargeted Self-Revision Is Unreliable

To examine whether untargeted revision of the entire reasoning chain can address these errors, we evaluate generic Self-Revision on RealWorldQA, where the same MLLM is provided with the original image, question, initial reasoning chain, and answer and is asked to reconsider and revise the complete reasoning process without explicit error localization or external visual evidence. The complete prompt is provided in Appendix E. As shown in Fig. 3, Self-Revision improves InternVL but degrades Qwen and Llama, indicating that such perceptual unfaithfulness is not merely attributable to stochastic sampling, but instead reflects systematic limitations in the visual perception of MLLMs (Li et al., 2025a; Chen et al., 2026b). It is therefore necessary to introduce independent and reliable visual evidence and explicitly localize the spatial evidence units that require correction.

These analyses suggest that improving final-answer accuracy through perceptually faithful reasoning requires locating specific spatial evidence units in the CoT that conflict with the visual input and providing their locations and verification evidence for targeted regeneration.

3 Method

Motivated by the above analyses, we propose a training-free framework for spatial reasoning verification and correction that locates and corrects perceptually unfaithful spatial evidence units, thereby improving perceptual faithfulness and final-answer accuracy. As illustrated in Fig. 4, given an image I and a question q, an MLLM first generates an initial reasoning chain and answer. The framework then extracts spatial evidence units to construct a SEG, verifies each using visual evidence assessed for reliability, locates the earliest unit contradicted by reliable evidence, and guides the model to revise the affected subsequent reasoning and final answer.

3.1 Spatial Evidence Graph Construction

Spatial judgments in natural-language CoT are often distributed across different reasoning steps, making them difficult to verify independently and trace back to their origins when errors are detected. To address this issue, we explicitly convert these judgments into a Spatial Evidence Graph (SEG). The construction process consists of three steps: extracting spatial evidence units from the reasoning chain, mapping them into a unified graph structure, and associating them with the visual evidence required for subsequent verification.

Given an initial reasoning chain $C = \{c_1, c_2, \ldots, c_n\}$, we prompt an MLLM to extract spatial evidence units from each reasoning step across four types: object existence, absolute image position, 2D relative spatial relations, and relative depth. Each unit retains its source step, enabling unsupported evidence to be localized in the original CoT. We organize these units into a SEG $\mathcal{G} = (\mathcal{V}, \mathcal{E}, \mathcal{A})$, where $\mathcal{V}$ contains visual entity nodes and an image-reference node, $\mathcal{E}$ denotes directed spatial-relation edges, and $\mathcal{A}$ stores evidence types, source steps, and visual evidence. Object

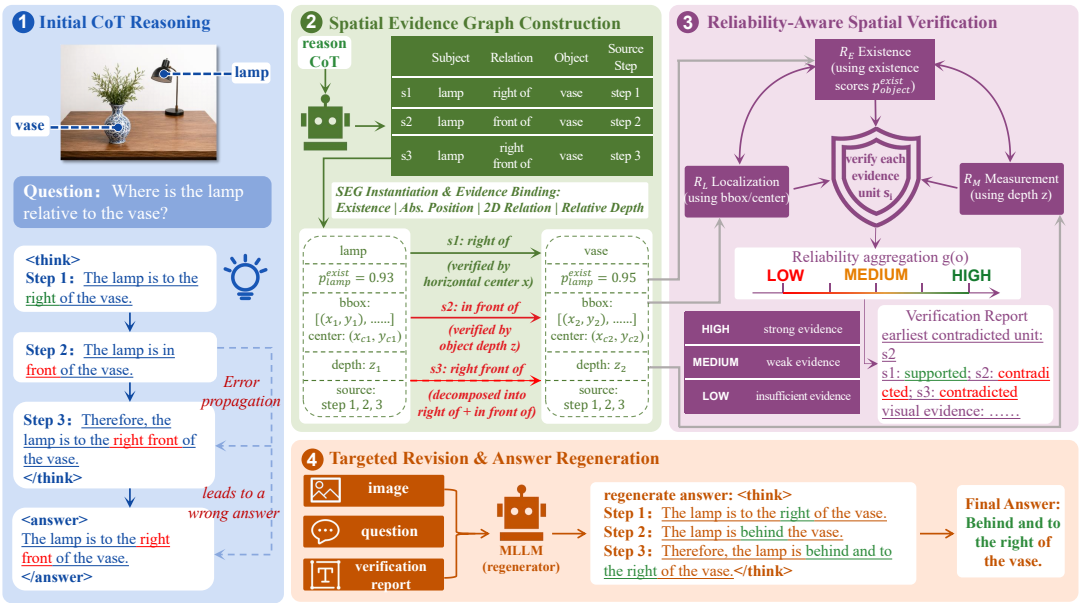

Figure 4: Overview of our process-oriented spatial reasoning correction framework. SEG structures intermediate spatial evidence, SERA assesses visual evidence reliability, and the earliest contradicted evidence unit guides targeted reasoning and answer regeneration.

existence is represented as an entity-node attribute, while absolute positions and inter-object relations are represented as directed edges. Each unit is formally represented as

$$s_m = \langle o_i, r_m, o_j, t_m, k_m \rangle ,$$

where o_i and o_j denote the entities or reference node involved in the evidence unit, r_m denotes the encoded spatial relation, t_m denotes the evidence type, and k_m records the source reasoning step.

Finally, we associate visual evidence by evidence type. For each entity, Grounding DINO (Liu et al., 2024a) provides candidate boxes and confidence scores, from which we compute the existence score $p_{\text{yes}}(o)$ following FaithAct. Bounding-box coordinates support absolute-position and 2D relation units. For depth relations, SAM2 (Ravi et al., 2025) provides object masks, and a monocular depth estimator (Yang et al., 2024) computes depth statistics within them. The resulting SEG links its nodes and edges to the evidence required for reliability assessment and verification. Extraction prompts and details are provided in Appendix B.

3.2 Reliability-Aware Spatial Verification

The SEG specifies the spatial evidence units to be verified and associates them with the corresponding visual entities and evidence. However, in challenging cases involving small objects, occlusion, cluttered backgrounds, or ambiguous boundaries, the associated visual observations may exhibit substantial uncertainty. For example, object detection may produce low-confidence or incomplete bounding boxes, while depth estimation may be affected by segmentation boundary errors and depth variations within the object region. Treating all visual evidence as equally reliable in such cases may lead to overconfident verification decisions and introduce new errors into subsequent reasoning revision. We therefore introduce Spatial Evidence Reliability Assessment (SERA), which evaluates whether the relevant visual evidence is sufficiently reliable to support a decisive judgment before verifying each spatial evidence unit. This process consists of entity-level evidence reliability assessment and evidence-unit-level spatial verification.

For each visual entity o, SERA evaluates three complementary aspects of its evidence: existence certainty, localization clarity, and geometric-measurement stability, denoted by $R_E(o)$, $R_L(o)$, and $R_M(o)$, respectively. Let $p_{\text{yes}}(o) \in [0, 1]$ denote the image-level probability that entity o is present, obtained during SEG construction. We define existence reliability as

$$R_E(o) = 2\,|p_{\text{yes}}(o) - 0.5| \,.$$

Localization reliability measures whether the entity is localized unambiguously. Let s_1 and s_2 denote the top two raw grounding scores produced by Grounding DINO for entity o. We define

$$R_L(o) = \min\left(\sigma(s_1), \sigma(s_1 - s_2)\right) ,$$

where the first term measures the confidence of the top-ranked candidate, while the second mea-

sures its score margin over the second-ranked candidate. A small margin indicates that multiple candidate locations have similar scores and that the localization may therefore be ambiguous. Here, $\sigma(\cdot)$ denotes the sigmoid function.

Geometric-measurement reliability evaluates the stability of the visual measurements used for evidence unit verification. For evidence units that do not involve relative depth, no additional geometric measurement is required, and we therefore set $R_M(o) = 1$. For relative-depth evidence units, measurement reliability depends on both mask-area sufficiency and depth consistency:

$$R_M(o) = \begin{cases} 1, & \text{for non-depth evidence units,} \\ a_{\text{mask}}(o)\, d_{\text{stable}}(o). \end{cases}$$

$$a_{\text{mask}}(o) = \sigma\left(\log_{10}\left(\max(|M_o|, 1)\right) - \theta_m\right),$$

$$d_{\text{stable}}(o) = \sigma\left(\theta_d - \text{Std}(D_o)\right).$$

Here, M_o denotes the segmentation mask of entity o, and D_o denotes the depth values within the corresponding masked region. A larger valid mask region and lower within-region depth variance indicate a more stable depth measurement.

The three reliability components are aggregated into an entity-level evidence reliability score using a weighted geometric mean:

$$g(o) = R_E(o)^{\alpha} R_L(o)^{\beta} R_M(o)^{\gamma}, \quad \alpha+\beta+\gamma = 1.$$

This aggregation substantially reduces the overall reliability when any critical evidence component has a low value, while α, β, and γ control the relative contributions of the three components. Based on $g(o)$, the evidence associated with each entity is divided into three reliability tiers:

$$\text{tier}(o) = \begin{cases} \text{HIGH}, & g(o) \geq \tau_h, \\ \text{MEDIUM}, & \tau_l \leq g(o) < \tau_h, \\ \text{LOW}, & g(o) < \tau_l. \end{cases}$$

We set $\tau_h = 0.75$ and $\tau_l = 0.45$. A positive object-existence unit is marked as SUPPORTED if $R_E(o) \geq \tau_h$ and $p_{\text{yes}}(o) > 0.5$, and CONTRADICTED if $R_E(o) \geq \tau_h$ and $p_{\text{yes}}(o) < 0.5$; labels are reversed for negative units. Any existence unit with $R_E(o) < \tau_h$ is marked as INCONCLUSIVE.

After verification, we sort the results by source step and locate the earliest spatial evidence unit contradicted by reliable visual evidence. Its source step, result, and visual evidence form a verification report, which is provided with the original image and question to the same MLLM to revise the judgment and regenerate the affected reasoning and final answer. If no reliable contradiction is found, the original reasoning and answer are retained. Detailed verification rules and the regeneration prompt are provided in Appendix C.

4 Experiments

4.1 Experimental Setup

Datasets and models. We evaluate our method on five benchmarks: 60 samples from LLaVA-Bench-in-the-Wild (Liu et al., 2023), 765 samples from RealWorldQA (AI, 2024), 3,000 samples from the POPE split (Li et al., 2023), 12,578 samples from the GQA balanced test-dev (Hudson and Manning, 2019), and 96 samples from MMHal-Bench (Sun et al., 2024). These benchmarks cover open-ended visual question answering, real-world scene understanding, object-existence hallucination, and spatial-relation reasoning. Evaluation protocols for different datasets are provided in Appendix D. We use Qwen3-VL-8B-Instruct (Bai et al., 2025), InternVL3.5-8B (Wang et al., 2025a), and Llama-3.2-11B-Vision-Instruct (Grattafiori et al., 2024) as backbone models.

Baselines and metrics. We compare our method with Vanilla, SpatialPIN (Ma et al., 2024), ByDeWay (Roy et al., 2025), SoM (Yang et al., 2023), GoM (Frisoni et al., 2026), and FaithAct (Li et al., 2026a). All methods use identical samples and evaluation procedures, with final-answer accuracy as the primary metric. We also use Spatial Evidence Faithfulness (SEF) to assess intermediate reasoning. For sample i, let S_i and C_i denote the numbers of SUPPORTED and CONTRADICTED units, respectively, and define $\text{SEF}_i = S_i/(S_i + C_i)$.

4.2 Main Results

To evaluate the overall effectiveness of our framework and its applicability across models and datasets, we compare it with Vanilla reasoning and several inference-time spatial augmentation and verification methods on three MLLMs and five benchmarks. As shown in Tab. 2, our method achieves the best performance in 11 of the 15 model–dataset settings. Specifically, the average accuracy increases from 64.33% to 70.59% for Qwen, from 56.11% to 68.55% for InternVL, and from 63.55% to 67.68% for Llama. In contrast, the

Model + Method	LLaVA-Bench (%)	RealWorldQA (%)	POPE (%)	GQA (%)	MMHal (%)	Average (%)
Qwen + Vanilla	63.33	63.66	74.90	56.21	63.54	64.33
+ SpatialPIN	58.33	64.44	85.67	48.33	63.54	64.06
+ ByDeWay	65.00	65.36	82.90	56.49	66.67	67.28
+ SoM	60.00	64.18	85.43	**60.10**	63.54	66.65
+ GoM	56.67	53.20	85.43	33.88	54.17	56.67
+ FaithAct	53.33	46.54	79.67	55.13	64.58	59.85
+ **Ours**	**71.67**	**66.93**	**86.33**	57.20	**70.83**	**70.59**
InternVL + Vanilla	53.33	48.63	75.60	43.62	59.38	56.11
+ SpatialPIN	45.00	60.52	80.83	51.18	55.21	58.55
+ ByDeWay	56.67	44.18	85.27	55.22	60.42	60.35
+ SoM	48.33	56.73	79.30	59.92	47.92	58.44
+ GoM	46.67	56.73	86.23	47.94	42.71	56.06
+ FaithAct	41.67	60.65	65.63	49.80	47.92	53.13
+ **Ours**	**60.00**	**66.14**	**88.57**	**60.35**	**67.71**	**68.55**
Llama + Vanilla	58.33	54.90	81.30	69.06	54.17	63.55
+ SpatialPIN	48.33	45.88	84.73	66.62	58.33	60.78
+ ByDeWay	51.67	56.60	86.27	60.26	55.21	62.00
+ SoM	41.67	52.81	82.80	60.02	**63.54**	60.17
+ GoM	41.67	43.01	**86.67**	63.00	47.92	56.45
+ FaithAct	40.00	58.43	86.40	**75.08**	53.13	62.61
+ **Ours**	**65.00**	**61.18**	85.30	71.72	55.21	**67.68**

Table 2: Performance comparison across five multimodal reasoning benchmarks using Qwen3-VL-8B-Instruct, InternVL3.5-8B, and Llama-3.2-11B-Vision-Instruct. Bold and underlined values denote the best and second-best results, respectively, within each model–dataset setting.

Dataset	Spatial Evidence Faithfulness (% ↑)		Final-answer Accuracy (% ↑)
	Human Eval.	Model Eval.	
RealWorldQA	82.12 → **92.47** (+10.35)	81.79 → **91.40** (+9.61)	45.00 → **57.00** (+12.00)
GQA	90.94 → **96.70** (+5.76)	90.03 → **95.60** (+5.57)	62.00 → **69.00** (+7.00)

Table 3: Relationship between spatial evidence faithfulness and final-answer accuracy on 200-example subsets of RealWorldQA and GQA. Values before and after → correspond to Vanilla and our method, respectively.

other methods exhibit more variable gains across models and benchmarks. These results demonstrate that our method provides consistent improvements across different backbones and datasets, indicating that explicitly verifying and correcting intermediate spatial evidence is more effective than merely augmenting the initial spatial information.

4.3 Reasoning Faithfulness

To examine whether our method improves perceptual faithfulness, we evaluate SEF on fixed subsets of RealWorldQA and GQA and analyze its change over the reasoning process. As shown in Tab.3, both human and automatic evaluations show an upward trend in SEF, accompanied by improvements in final-answer accuracy. Figure 5 shows that Vanilla's SEF steadily declines as reasoning progresses, whereas our method remains consistently higher and improves SEF@100 by 8.97% on GQA. These results demonstrate that the framework improves both the perceptual faithfulness of intermediate reasoning and final-answer accuracy.

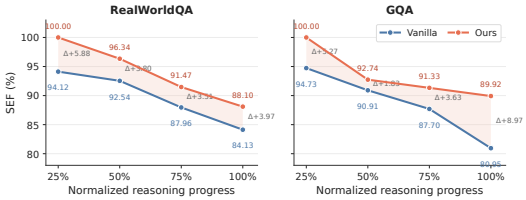

Figure 5: Cumulative spatial evidence faithfulness on fixed 500-sample subsets of RealWorldQA and GQA using InternVL3.5-8B.

Backbone	Full	w/o SEG (Δ)	w/o SERA (Δ)
Qwen3-VL-8B	**66.93**	63.92 (−3.01)	62.88 (−4.05)
InternVL3.5-8B	**66.14**	63.01 (−3.13)	61.96 (−4.18)
Llama-3.2-11B	**61.18**	58.56 (−2.62)	57.65 (−3.53)

Table 4: Ablation study of SEG and SERA on RealWorldQA across multiple MLLMs.

4.4 Ablation Studies

Component ablation. To assess the contributions of the two core modules, we remove SEG and SERA separately. In w/o SEG, spatial evidence units are processed as a flat list without constructing a graph connecting entities, relations, visual evidence, and source steps. In w/o SERA, SEG and visual evidence collection are retained, but reliability assessment and gating are removed, allowing direct evidence use for verification and correction. As shown in Tab. 4, removing SEG and SERA re-

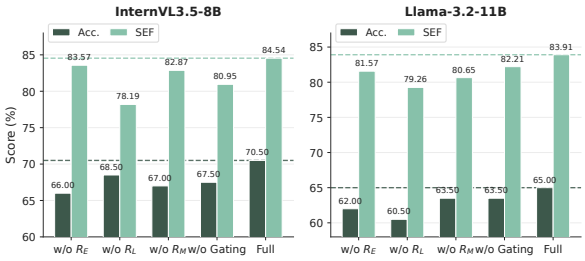

Figure 6: Fine-grained ablation of SERA on a fixed 200-sample subset of RealWorldQA.

Setting	τ_l	τ_h	SEF (%)	Acc. (%)
Loose	0.35	0.65	84.04	51
Default	0.45	0.75	**89.36**	**55**
Strict	0.55	0.85	86.17	52

Table 5: Sensitivity of SERA to its reliability thresholds on a fixed 100-sample subset of RealWorldQA using Qwen3-VL-8B-Instruct.

duces average accuracy across the three backbones by 2.92 and 3.92 percentage points, respectively, confirming the contributions of structured evidence organization and reliability-aware verification.

Fine-grained SERA ablation. To analyze SERA's components, we separately remove R_E, R_L, R_M, and reliability-aware gating. In w/o R_E, only R_L and R_M are aggregated with renormalized weights. In w/o R_L or w/o R_M, the corresponding visual evidence is retained but excluded from reliability estimation. In w/o Gating, all components remain, but reliability tiers no longer determine whether verification is decisive. As shown in Fig. 6, each removal reduces accuracy and SEF, with R_L having the largest impact, confirming their complementary roles.

Threshold sensitivity. To assess SERA's threshold sensitivity, we compare loose, default, and strict settings. As shown in Tab. 5, the default setting achieves the highest SEF and accuracy. Loose thresholds allow noisy evidence to trigger correction, whereas strict thresholds yield more inconclusive units. The default thresholds better balance correction coverage and evidence reliability.

4.5 Human Validation of Intermediate Components

To validate the automatic components, we randomly sampled 50 CoT responses each from RealWorldQA and GQA. Human annotators identify spatial evidence units and their source steps for strict exact-match evaluation of the extractor, and label the resulting 291 units as *Supported*, *Contradicted*, or *Inconclusive* for verifier evaluation. As shown in Tab.6, the extractor achieves F1 scores of 91.99% and 91.72% on the two datasets, while the verifier achieves 94.85% three-way accuracy and 81.76% Macro-F1, with 95.47% decisive accuracy at 91.07% coverage, indicating high agreement with human judgments, providing a reliable basis for subsequent correction.

(a) Spatial Evidence Extraction

Dataset	Precision (%)	Recall (%)	F1 (%)
RealWorldQA	89.19	94.96	91.99
GQA	88.89	94.74	91.72

(b) Automatic Spatial Verification

Dataset	3-way Acc.	F1-S	F1-C	F1-I	Macro-F1	Dec. Acc.	Coverage
RealWorldQA	94.96	98.20	58.82	92.31	83.11	95.00	85.61
GQA	94.74	97.81	58.82	76.92	77.85	95.86	96.05

Table 6: Human validation of the spatial evidence extractor and verifier. Panel (a) reports extraction quality under strict exact matching of all evidence fields and source steps. Panel (b) reports verification quality. S, C, and I denote *Supported*, *Contradicted*, and *Inconclusive*. Dec. Acc. is accuracy on human-decidable units, and Coverage is the proportion assigned a decisive label.

Method	Performance	Inference Efficiency	
	Accuracy (%, ↑)	E2E Time (s)	Time/Tok. (ms)
Vanilla	53.00	0.8943	1.4425
SpatialPIN	52.00 (↓1.00)	1.3151 (×1.47)	1.0950 (×0.76)
ByDeWay	58.00 (↑5.00)	1.3155 (×1.47)	1.0262 (×0.71)
SoM	59.00 (↑6.00)	0.9626 (×1.08)	1.4232 (×0.99)
GoM	50.00 (↓3.00)	0.9384 (×1.05)	1.5132 (×1.05)
FaithAct	58.00 (↑5.00)	1.2566 (×1.41)	1.0425 (×0.72)
Ours	**61.00** (↑8.00)	2.5095 (×2.81)	3.3592 (×2.33)

Table 7: Performance and efficiency on a 100-sample GQA subset using InternVL3.5-8B. E2E Time denotes average end-to-end inference latency, while Time/Tok. denotes the latency normalized by output length.

4.6 Efficiency and Scope Analysis

To assess inference cost and cross-task generality, we evaluate efficiency on a fixed 100-sample GQA subset using InternVL3.5-8B and transfer to ScienceQA and MathVista across three backbones. All latency measurements use identical hardware and software settings on eight NVIDIA GeForce RTX 4090 GPUs.

Inference efficiency. As shown in Tab. 7, although our method incurs higher overall latency, its absolute runtime remains on the order of seconds while delivering the largest accuracy gain of 8.00

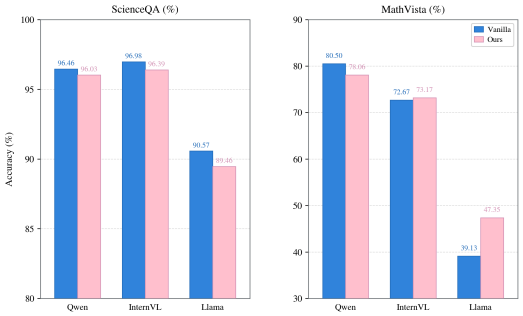

Figure 7: Transfer analysis on ScienceQA and MathVista. Results are reported as final-answer accuracy.

percentage points. Moreover, it does not modify the underlying generation function or decoding procedure of the MLLM. Thus, our method achieves a substantial performance improvement with manageable test-time overhead while preserving the original generation mechanism.

Transfer beyond spatial reasoning. As shown in Fig. 7, the maximum performance decrease on ScienceQA is only 1.11 percentage points. On MathVista, Qwen decreases by 2.44 points, whereas InternVL and Llama improve by 0.50 and 8.22 points, respectively. Overall, our method largely preserves the models' performance on broader multimodal tasks and provides additional gains in some settings.

4.7 Complementarity with Inference-Time Spatial Augmentation

To evaluate whether our process-oriented spatial reasoning correction complements inference-time spatial augmentation for final-answer performance, we combine it with SpatialPIN. As shown in Tab.8, the combination achieves an average accuracy of 65.45%, outperforming SpatialPIN alone (56.95%) and our method alone (64.75%). It also outperforms both methods across all three backbones. These results demonstrate the complementarity between inference-time spatial augmentation and process-oriented spatial reasoning correction.

5 Related Work

5.1 Spatial Reasoning in Multimodal LLMs

Existing methods for MLLM spatial reasoning mainly use training-based enhancement or inference-time augmentation. Training-based methods construct spatial instruction data or introduce region- and depth-aware representations (Chen et al., 2024; Cheng et al., 2024; Sun et al., 2025b; Ogezi and Shi, 2025). Inference-time methods provide depth cues, 3D priors, visual marks, or structured scene representations (Ma et al., 2024; Roy et al., 2025; Yang et al., 2023; Frisoni et al., 2026). However, they enhance spatial knowledge without verifying whether intermediate judgments are visually supported. Our method instead extracts and verifies spatial evidence units from CoT and traces unsupported units to their source steps.

Method	Qwen	InternVL	Llama	Average
Vanilla	63.66	48.63	54.90	55.73
SpatialPIN	64.44	60.52	45.88	56.95
Ours	66.93	66.14	61.18	64.75
SpatialPIN + Ours	**67.71**	**66.41**	**62.22**	**65.45**

Table 8: Performance of SpatialPIN, our process-oriented correction, and their combination on RealWorldQA.

5.2 Faithful Reasoning and Verification

Recent methods improve multimodal faithfulness through decoding correction, reasoning verification, or post-hoc grounding. Decoding methods suppress unsupported language priors by adjusting output distributions or strengthening visual grounding (Wang et al., 2024; Ghosh et al., 2025), while verifier-based and post-hoc methods check reasoning trajectories against localized visual evidence (Sun et al., 2025a; Yi and Shang, 2025). FaithAct uses the visual faithfulness of intermediate reasoning to guide correction (Li et al., 2026a). However, these methods neither represent inter-object spatial relations as verifiable evidence units nor assess the reliability of corrective visual evidence. We address both limitations through SEG-based evidence tracing and SERA-based reliability-aware verification.

6 Conclusion

We propose a modular and training-free framework for perceptually faithful spatial reasoning in MLLMs. The SEG structures intermediate spatial evidence units and preserves their source steps, while SERA determines whether existence, localization, and geometric evidence is sufficiently reliable for verification. The framework then corrects the earliest contradicted evidence unit and regenerates the affected reasoning steps to prevent error propagation. Experiments across three representative MLLMs and five benchmarks show that our method achieves an average accuracy of 68.94%, outperforming the compared baselines by 8.55 percentage points on average. These results demon-

strate that evidence-level verification provides an effective approach to improving spatial reasoning.

Limitations

Although in this work we present a systematic and training-free framework for verifying and correcting spatial reasoning in MLLMs, it still has several limitations.

First, the framework relies on explicit CoT and can verify only the spatial evidence successfully extracted from the generated reasoning. Spatial errors that remain implicit or are omitted from the CoT cannot be directly localized or corrected, while non-spatial reasoning errors fall beyond the scope of the current framework. Second, our experiments mainly focus on static-image question-answering benchmarks and three open-source MLLM backbones. Its effectiveness in video understanding, multi-view reasoning, proprietary MLLMs, and closed-loop embodied interaction therefore remains to be investigated. Future work will explore the identification of implicit spatial evidence and extend the framework to a broader range of models, tasks, and dynamic embodied environments.

References

X AI. 2024. Grok-1.5 vision preview.

Shuai Bai, Yuxuan Cai, Ruizhe Chen, Keqin Chen, Xionghui Chen, Zesen Cheng, Lianghao Deng, Wei Ding, Chang Gao, Chunjiang Ge, and 1 others. 2025. Qwen3-vl technical report. *arXiv preprint arXiv:2511.21631*.

Boyuan Chen, Zhuo Xu, Sean Kirmani, Brain Ichter, Dorsa Sadigh, Leonidas Guibas, and Fei Xia. 2024. Spatialvlm: Endowing vision-language models with spatial reasoning capabilities. In *Proceedings of the IEEE/CVF Conference on Computer Vision and Pattern Recognition*, pages 14455–14465.

Jiawei Chen, Simin Huang, Jiawei Du, Shuaihang Chen, Yu Tian, Mingjie Wei, Chao Yu, and Zhaoxia Yin. 2026a. Tex3d: Objects as attack surfaces via adversarial 3d textures for vision-language-action models. *arXiv preprint arXiv:2604.01618*.

Jiawei Chen, Yang Yang, Chao Yu, Yu Tian, Zhi Cao, Xue Yang, Linghao Li, Hang Su, and Zhaoxia Yin. 2026b. Red teaming large reasoning models. In *Proceedings of the 64th Annual Meeting of the Association for Computational Linguistics (Volume 1: Long Papers)*, pages 22559–22591.

An-Chieh Cheng, Hongxu Yin, Yang Fu, Qiushan Guo, Ruihan Yang, Jan Kautz, Xiaolong Wang, and Sifei Liu. 2024. Spatialrgpt: Grounded spatial reasoning in vision-language models. *Advances in Neural Information Processing Systems*, 37:135062–135093.

Erik Daxberger, Nina Wenzel, David Griffiths, Haiming Gang, Justin Lazarow, Gefen Kohavi, Kai Kang, Marcin Eichner, Yinfei Yang, Afshin Dehghan, and 1 others. 2025. Mm-spatial: Exploring 3d spatial understanding in multimodal llms. In *Proceedings of the IEEE/CVF International Conference on Computer Vision*, pages 7395–7408.

Renhua Ding, Xiao Yang, Zhengwei Fang, Jun Luo, Kun He, and Jun Zhu. 2025. Invisible to humans, triggered by agents: Stealthy jailbreak attacks on mobile vision-language agents. *arXiv preprint arXiv:2510.07809*.

Giacomo Frisoni, Lorenzo Molfetta, Mattia Buzzoni, and Gianluca Moro. 2026. Graph-of-mark: Promote spatial reasoning in multimodal language models with graph-based visual prompting. *arXiv preprint arXiv:2603.06663*.

Mohsen Gholami, Ahmad Rezaei, Zhou Weimin, Sitong Mao, Shunbo Zhou, Yong Zhang, and Mohammad Akbari. 2025. Spatial reasoning with vision-language models in ego-centric multi-view scenes. *arXiv preprint arXiv:2509.06266*.

Sreyan Ghosh, Chandra Kiran Evuru, Sonal Kumar, Utkarsh Tyagi, Oriol Nieto, Zeyu Jin, and Dinesh Manocha. 2025. Visual description grounding reduces hallucinations and boosts reasoning in lvlms. In *International Conference on Learning Representations*, volume 2025, pages 66510–66547.

Aaron Grattafiori, Abhimanyu Dubey, Abhinav Jauhri, Abhinav Pandey, Abhishek Kadian, Ahmad Al-Dahle, Aiesha Letman, Akhil Mathur, Alan Schelten, Alex Vaughan, and 1 others. 2024. The llama 3 herd of models. *arXiv preprint arXiv:2407.21783*.

Jiacheng Hua, Yishu Yin, Yuhang Wu, Tai Wang, Yifei Huang, and Miao Liu. 2026. Unleashing spatial reasoning in multimodal large language models via textual representation guided reasoning. In *Proceedings of the 64th Annual Meeting of the Association for Computational Linguistics (Volume 1: Long Papers)*, pages 13616–13637.

Drew A Hudson and Christopher D Manning. 2019. Gqa: A new dataset for real-world visual reasoning and compositional question answering. In *Proceedings of the IEEE/CVF conference on computer vision and pattern recognition*, pages 6700–6709.

Jingjing Jiang, Chao Ma, Xurui Song, Hanwang Zhang, and Jun Luo. 2025. Corvid: Improving multimodal large language models towards chain-of-thought reasoning. In *Proceedings of the IEEE/CVF International Conference on Computer Vision*, pages 3034–3046.

Juntao Jiang, Jiangning Zhang, Yali Bi, Jinsheng Bai, Weixuan Liu, Weiwei Jin, Zhucun Xue, Yong Liu, Xiaobin Hu, and Shuicheng Yan. 2026.

M3cotbench: Benchmark chain-of-thought of mllms in medical image understanding. *arXiv preprint arXiv:2601.08758*.

Jiayi Kuang, Ying Shen, Jingyou Xie, Haohao Luo, Zhe Xu, Ronghao Li, Yinghui Li, Xianfeng Cheng, Xika Lin, and Yu Han. 2025. Natural language understanding and inference with mllm in visual question answering: A survey. *ACM Computing Surveys*, 57(8):1–36.

Jiaze Li, Hao Yin, Wenhui Tan, Jingyang Chen, Boshen Xu, Yuxun Qu, Yijing Chen, Jianzhong Ju, Zhenbo Luo, and Jian Luan. 2025a. Revisor: Beyond textual reflection, towards multimodal introspective reasoning in long-form video understanding. *arXiv preprint arXiv:2511.13026*.

Junxian Li, Xinyue Xu, Sai Ma, Di Zhang, and Sichao Li. 2026a. Faithful-first reasoning, planning, and acting for multimodal llms. In *Findings of the Association for Computational Linguistics: ACL 2026*, pages 6777–6793.

Pengteng Li, Pinhao Song, Wuyang Li, Weiyu Guo, Huizai Yao, Yijie Xu, Dugang Liu, and Hui Xiong. 2025b. See&trek: Training-free spatial prompting for multimodal large language model. *arXiv preprint arXiv:2509.16087*.

Yifan Li, Yifan Du, Kun Zhou, Jinpeng Wang, Xin Zhao, and Ji-Rong Wen. 2023. Evaluating object hallucination in large vision-language models. In *Proceedings of the 2023 conference on empirical methods in natural language processing*, pages 292–305.

Zongzhao Li, Zongyang Ma, Mingze Li, Songyou Li, Yu Rong, Tingyang Xu, Ziqi Zhang, Deli Zhao, and Wenbing Huang. 2026b. Star-r1: Multi-view spatial transformation reasoning by reinforcing multimodal llms. In *Proceedings of the IEEE/CVF Conference on Computer Vision and Pattern Recognition*, pages 12041–12051.

Haotian Liu, Chunyuan Li, Qingyang Wu, and Yong Jae Lee. 2023. Visual instruction tuning. *Advances in neural information processing systems*, 36:34892–34916.

Shilong Liu, Zhaoyang Zeng, Tianhe Ren, Feng Li, Hao Zhang, Jie Yang, Qing Jiang, Chunyuan Li, Jianwei Yang, Hang Su, and 1 others. 2024a. Grounding dino: Marrying dino with grounded pre-training for open-set object detection. In *European conference on computer vision*, pages 38–55. Springer.

Shuyuan Liu, Jiawei Chen, Shouwei Ruan, Hang Su, and Zhaoxia Yin. 2024b. Exploring the robustness of decision-level through adversarial attacks on llm-based embodied models. In *Proceedings of the 32nd ACM international conference on multimedia*, pages 8120–8128.

Weijiang Lv, Yaoxuan Feng, Xiaobo Xia, Jiayu Wang, Yan Jing, Wenchao Chen, and Bo Chen. 2026. Spd-faith bench: Diagnosing and improving faithfulness in chain-of-thought for multimodal large language models. *arXiv preprint arXiv:2602.07833*.

Chenyang Ma, Kai Lu, Ta-Ying Cheng, Niki Trigoni, and Andrew Markham. 2024. Spatialpin: Enhancing spatial reasoning capabilities of vision-language models through prompting and interacting 3d priors. *Advances in neural information processing systems*, 37:68803–68832.

Jinlong Ma, Yu Zhang, Xuefeng Bai, Kehai Chen, Yuwei Wang, Zeming Liu, Jun Yu, and Min Zhang. 2026. Beyond unimodal shortcuts: Mllms as cross-modal reasoners for grounded named entity recognition. *arXiv preprint arXiv:2602.04486*.

Fanqing Meng, Jin Wang, Chuanhao Li, Quanfeng Lu, Hao Tian, Tianshuo Yang, Jiaqi Liao, Xizhou Zhu, Jifeng Dai, Yu Qiao, and 1 others. 2025. Mmiu: Multimodal multi-image understanding for evaluating large vision-language models. In *International Conference on Learning Representations*, volume 2025, pages 38405–38453.

Michael Ogezi and Freda Shi. 2025. Spare: Enhancing spatial reasoning in vision-language models with synthetic data. In *Proceedings of the 63rd Annual Meeting of the Association for Computational Linguistics (Volume 1: Long Papers)*, pages 7855–7875.

Nikhila Ravi, Valentin Gabeur, Yuan-Ting Hu, Ronghang Hu, Chaitanya Ryali, Tengyu Ma, Haitham Khedr, Roman Rädle, Chloe Rolland, Laura Gustafson, and 1 others. 2025. Sam 2: Segment anything in images and videos. In *International Conference on Learning Representations*, volume 2025, pages 28085–28128.

Rajarshi Roy, Devleena Das, Ankesh Banerjee, Arjya Bhattacharjee, Kousik Dasgupta, and Subarna Tripathi. 2025. Bydeway: Boost your multimodal llm with depth prompting in a training-free way. In *Proceedings of the IEEE/CVF International Conference on Computer Vision*, pages 6058–6064.

Linzhuang Sun, Hao Liang, Jingxuan Wei, Bihui Yu, Tianpeng Li, Fan Yang, Zenan Zhou, and Wentao Zhang. 2025a. Mm-verify: Enhancing multimodal reasoning with chain-of-thought verification. In *Proceedings of the 63rd Annual Meeting of the Association for Computational Linguistics (Volume 1: Long Papers)*, pages 14100–14115.

Xuefei Sun, Doncey Albin, Cecilia Mauceri, Destin Woods, and Chris Heckman. 2025b. Spatial-llava: Enhancing large language models with spatial referring expressions for visual understanding. In *ICRA 2025 Workshop: Human-Centered Robot Learning in the Era of Big Data and Large Models*.

Zhiqing Sun, Sheng Shen, Shengcao Cao, Haotian Liu, Chunyuan Li, Yikang Shen, Chuang Gan, Liangyan Gui, Yu-Xiong Wang, Yiming Yang, and 1 others.

2024. Aligning large multimodal models with factually augmented rlhf. In *Findings of the Association for Computational Linguistics: ACL 2024*, pages 13088–13110.

Chenxi Wang, Xiang Chen, Ningyu Zhang, Bozhong Tian, Haoming Xu, Shumin Deng, and Huajun Chen. 2024. Mllm can see? dynamic correction decoding for hallucination mitigation. *arXiv preprint arXiv:2410.11779*.

Weiyun Wang, Zhangwei Gao, Lixin Gu, Hengjun Pu, Long Cui, Xingguang Wei, Zhaoyang Liu, Linglin Jing, Shenglong Ye, Jie Shao, and 1 others. 2025a. Internvl3. 5: Advancing open-source multimodal models in versatility, reasoning, and efficiency. *arXiv preprint arXiv:2508.18265*.

Yuxin Wang, Lei Ke, Boqiang Zhang, Tianyuan Qu, Hanxun Yu, Zhenpeng Huang, Meng Yu, Dan Xu, and Dong Yu. 2025b. N3d-vlm: Native 3d grounding enables accurate spatial reasoning in vision-language models. *arXiv preprint arXiv:2512.16561*.

Jianwei Yang, Hao Zhang, Feng Li, Xueyan Zou, Chunyuan Li, and Jianfeng Gao. 2023. Set-of-mark prompting unleashes extraordinary visual grounding in gpt-4v. *arXiv preprint arXiv:2310.11441*.

Lihe Yang, Bingyi Kang, Zilong Huang, Zhen Zhao, Xiaogang Xu, Jiashi Feng, and Hengshuang Zhao. 2024. Depth anything v2. *Advances in Neural Information Processing Systems*, 37:21875–21911.

Shixin Yi and Lin Shang. 2025. Corgi: Verified chain-of-thought reasoning with post-hoc visual grounding. *arXiv preprint arXiv:2508.00378*.

Jiahui Zhang, Yurui Chen, Yueming Xu, Ze Huang, Jilin Mei, Chunhui Chen, Yanpeng Zhou, Yu-Jie Yuan, Xinyue Cai, Guowei Huang, and 1 others. 2026. From flatland to space: Teaching vision-language models to perceive and reason in 3d. *Advances in Neural Information Processing Systems*, 38.

Liangyu Zhong, Fabio Philipp Rosenthal, Joachim Sicking, Fabian Hüger, Thorsten Bagdonat, Hanno Gottschalk, and Leo Schwinn. 2026. Focus: Internal mllm representations for efficient fine-grained visual question answering. *Advances in Neural Information Processing Systems*, 38:96498–96535.

Fangrui Zhu, Hanhui Wang, Yiming Xie, Jing Gu, Tianye Ding, Jianwei Yang, and Huaizu Jiang. 2026. Struct2d: A perception-guided framework for spatial reasoning in mllms. *Advances in Neural Information Processing Systems*, 38:135805–135837.

A Discussion: Improving Accuracy through Perceptual Faithfulness

Our analysis reveals a strong association between perceptual faithfulness and final-answer accuracy: reasoning chains containing contradicted spatial evidence are substantially less accurate than fully faithful ones. This observation motivates our central hypothesis that improving the perceptual faithfulness of intermediate spatial reasoning can lead to more accurate final answers. To operationalize this idea, SEG makes spatial evidence units explicit and traceable to their source steps, while SERA determines whether the corresponding visual evidence is sufficiently reliable for verification and correction. By locating the earliest contradicted evidence unit and regenerating the affected reasoning, our framework reduces the propagation of visually unsupported spatial judgments. The consistent improvements in both Spatial Evidence Faithfulness and final-answer accuracy across datasets and backbones provide empirical support for this hypothesis. Moreover, the gains obtained by combining our framework with SpatialPIN suggest that enriching spatial information and improving the faithfulness of generated reasoning are complementary: the former provides additional spatial cues, whereas the latter verifies whether the intermediate evidence actually used by the model is consistent with the image. These findings indicate that perceptual faithfulness is not only a property for evaluating spatial reasoning, but also a practical direction for improving its final-answer accuracy.

B Spatial Evidence Extraction and SEG Construction Details

B.1 Step-wise Spatial Evidence Extraction

Given an initial reasoning chain $C = \{c_1, c_2, \ldots, c_n\}$, we process each reasoning step c_k to extract atomic spatial evidence units. Each extracted unit retains its source-step index k, allowing contradicted evidence to be traced back to its original position in the CoT. Following the definition in Sec. 3.1, the extractor covers four evidence types: object existence, absolute image position, 2D relative spatial relations, and relative depth.

Each spatial evidence unit is represented in the unified form

$$s_m = \langle o_i, r_m, o_j, t_m, k_m \rangle ,$$

where o_i and o_j denote the involved visual entities or the image-reference node, r_m denotes the encoded spatial relation, t_m denotes the evidence type, and k_m records the source reasoning step. For object-existence evidence, r_m records whether the entity is stated to be present or absent and o_j is not required. For absolute-position evidence, o_j is the image-reference node. For 2D relative and relative-depth evidence, o_i and o_j denote the two involved visual entities.

The extractor records only spatial evidence explicitly expressed in the corresponding reasoning step. A mere mention of an entity is not treated as an object-existence judgment, and hypothetical, conditional, interrogative, or uncertain expressions are not converted into decisive existence evidence. Composite spatial statements are decomposed into atomic units whenever they contain multiple relations. For example, "the lamp is to the right front of the vase" is decomposed into a 2D relation (`right_of`) and a relative-depth relation (`closer_than`).

Before graph construction, relation labels are canonicalized to the predefined vocabulary, while entity expressions required to distinguish different visual instances are preserved. Spatial statements appearing in different reasoning steps remain separate evidence units because their source-step indices differ. Only exact duplicate outputs within the same reasoning step are removed.

B.2 SEG Instantiation

The extracted evidence units are organized into a Spatial Evidence Graph $G = (V, E, A)$. The node set V contains visual entity nodes and an additional image-reference node. The edge set E contains directed spatial-relation edges. The attribute set A stores the evidence type, source-step index, and visual evidence associated with each node or edge.

Object-existence evidence is stored as an attribute of the corresponding entity node. Absolute-position evidence is represented as a directed edge from an entity node to the image-reference node. Both 2D relative relations and relative-depth relations are represented as directed edges between visual entity nodes. Each evidence record preserves its relation type and source-step index, enabling chronological ordering and subsequent error localization.

B.3 Visual Evidence Binding

For each visual entity involved in the extracted evidence units, Grounding DINO provides candidate bounding boxes and their confidence scores. The highest-scoring candidate is used as the primary localization result, while the top two raw grounding scores are retained for the localization-reliability computation defined in Sec. 3.2. Given a selected bounding box $b_o = (x_1, y_1, x_2, y_2)$, its center is

$$x_c(o) = \frac{x_1 + x_2}{2}, \qquad y_c(o) = \frac{y_1 + y_2}{2}.$$

The image-level existence probability $p_{\text{yes}}(o)$ is computed following FaithAct and is bound to the corresponding entity node for object-existence verification. Bounding-box coordinates and center locations provide the geometric evidence used for absolute-position and 2D relative-relation evidence units.

For relative-depth evidence units, the selected bounding box is used to prompt SAM2 to obtain an object mask. A monocular depth estimator then provides the depth values within the masked region, from which the object-level depth statistic and within-region stability information are computed. These measurements are bound to the corresponding depth-relation edge for subsequent reliability assessment and verification.

The resulting SEG therefore explicitly links each atomic spatial evidence unit to the visual observations required for verification. The reliability computation, verification decisions, and targeted correction report used by SERA are described separately in the reliability-aware verification appendix.

B.4 Spatial Evidence Extraction Prompt

Tab. 9 presents the prompt used to extract step-level spatial evidence units. The extractor is applied to each reasoning step, and the resulting units are subsequently combined to instantiate the SEG.

C Verification Report and Reasoning Regeneration Details

C.1 Spatial Evidence Verification Rules

For every visual entity involved in the reasoning chain, we first compute the predefined image-level existence judgment $J_E(o)$. This node-level judgment is used both to verify explicit object-existence evidence units and to check the entity-existence presuppositions of absolute-position, 2D relative-relation, and relative-depth evidence units. The node-level judgment itself does not introduce an additional existence evidence unit unless the initial CoT explicitly expresses the corresponding existence judgment.

Explicit object-existence evidence units are verified according to their extracted polarity. A `present` unit is marked as SUPPORTED when $J_E(o) =$ PRESENT and as CONTRADICTED when $J_E(o) =$ ABSENT. The decisions are reversed for an `absent` unit. If $J_E(o) =$ UNCERTAIN, the evidence unit is marked as INCONCLUSIVE. Verification of an existence unit depends only on the existence judgment determined by $R_E(o)$ and $p_{\text{yes}}(o)$, rather than on the aggregated entity-reliability tier.

For absolute image position, the bounding-box center is first normalized by the image width W and height H:

$$\tilde{x}_c(o) = \frac{x_c(o)}{W}, \qquad \tilde{y}_c(o) = \frac{y_c(o)}{H}.$$

The normalized center is then mapped to fixed horizontal and vertical partitions corresponding to `left`, `center`, and `right`, together with `top`, `center`, and `bottom`. Their combinations produce the nine supported image regions. The same frame-partition rules are used across all datasets and models.

Pairwise left–right and above–below relations are determined using bounding-box centers. Since the image-coordinate origin is located at the upper-left corner, a smaller x coordinate indicates a more leftward position, while a smaller y coordinate indicates a higher position:

$$o_i \texttt{ left_of } o_j \iff x_c(o_i) < x_c(o_j),$$

$$o_i \texttt{ above } o_j \iff y_c(o_i) < y_c(o_j).$$

The inverse comparisons are used for `right_of` and `below`. A fixed spatial margin is applied in implementation to avoid decisive judgments when two centers are nearly aligned.

The `near` relation is evaluated using the normalized 2D distance between the two object centers:

$$d_{\text{2D}}(o_i, o_j) = \left[\left(\frac{x_c(o_i) - x_c(o_j)}{W} \right)^2 + \left(\frac{y_c(o_i) - y_c(o_j)}{H} \right)^2 \right]^{1/2}.$$

A pair is considered near only when this distance is below the fixed threshold used in our implementation.

Prompt used for step-level spatial evidence extraction
Read the reasoning step below from a vision QA chain and extract all atomic spatial evidence units stated in this step. Do not use information from other reasoning steps and do not invent unstated relations. Each evidence unit must contain: {subject, relation, object, type, source_step}. Supported evidence types and relations: 1. **existence**: `present`, `absent`. Set `object` to null. 2. **absolute_position**: `left`, `right`, `top`, `bottom`, `center`, `top_left`, `top_right`, `bottom_left`, `bottom_right`. Set `object` to `image`. 3. **relative_2d**: `left_of`, `right_of`, `above`, `below`, `near`. 4. **relative_depth**: `closer_than`, `farther_than`. Map "in front of" to `closer_than` and "behind" to `farther_than`. Rules: - Copy the integer from the `[Step N]` label into `source_step`. - Preserve the entity expression needed to identify the intended visual instance, such as "the person on the left" or "the second car". - Extract an existence unit only when the step explicitly judges that an entity is present or absent. - Do not treat a mere entity mention as an existence judgment. - Do not convert hypothetical, conditional, interrogative, or uncertain expressions into decisive evidence units. - Decompose a statement containing multiple spatial relations into separate atomic evidence units. - Include repeated statements when they occur in different reasoning steps; their source steps are different. - If the step contains no spatial evidence, return an empty array. REASONING STEP: ###{CURRENT CoT STEP WITH [Step N] LABEL}### Return ONLY valid JSON with no Markdown formatting: { "evidence_units": [{ "subject": "the bus", "relation": "left_of", "object": "the car", "type": "relative_2d", "source_step": 1 }, { "subject": "the person on the left", "relation": "closer_than", "object": "the person on the right", "type": "relative_depth", "source_step": 1 }] }

Table 9: Prompt used to extract atomic spatial evidence units from each reasoning step.

For relative-depth relations, $z(o)$ denotes the mask-based object-level depth statistic computed after reversing the ordering of the raw inverse-depth prediction. Consequently, a smaller $z(o)$ indicates that an object is closer to the camera, whereas a larger value indicates that it is farther:

$$o_i \texttt{ closer_than } o_j \iff z(o_i) < z(o_j),$$

$$o_i \texttt{ farther_than } o_j \iff z(o_i) > z(o_j).$$

A fixed depth-difference margin is used to avoid decisive verification when the estimated depths are too similar. Monocular depth is compared only between objects in the same image.

For an absolute-position, 2D relative-relation, or relative-depth evidence unit, entity-existence presuppositions are checked before geometric verification. If any involved entity has $J_E(o) = \textsc{Absent}$, the evidence unit is marked as CONTRADICTED because its existence presupposition is violated. If any involved entity has $J_E(o) = \textsc{Uncertain}$, the evidence unit is marked as INCONCLUSIVE. Geometric verification is performed only when all involved entities have $J_E(o) = \textsc{Present}$. In this case, the corresponding geometric rule produces a SUPPORTED or CONTRADICTED result only when every involved entity is assigned to the HIGH tier. If any involved entity is assigned to the MEDIUM or LOW tier, the evidence unit is marked as INCONCLUSIVE.

C.2 Verification Report Construction

After evidence-level verification, we construct a verification record for each evidence unit containing its textual content, source reasoning step, verification result, evidence-specific reliability information, and precomputed visual judgment. All records are ordered by their source-step indices and, within the same step, by their order of occurrence in the initial CoT.

For each entity, the report retains its image-level existence score $p_{\text{yes}}(o)$, existence reliability $R_E(o)$, and precomputed existence judgment. For an explicit object-existence evidence unit, the report additionally retains its extracted polarity and source reasoning step. The existence judgment is defined

as

$$J_E(o) = \begin{cases} \text{PRESENT}, & \substack{R_E(o) \geq \tau_h \\ p_{\text{yes}}(o) > 0.5}, \\ \text{ABSENT}, & \substack{R_E(o) \geq \tau_h \\ p_{\text{yes}}(o) < 0.5}, \\ \text{UNCERTAIN}, & R_E(o) < \tau_h. \end{cases}$$

Here, PRESENT and ABSENT denote reliable presence and reliable absence, respectively, whereas UNCERTAIN indicates that the available existence evidence is insufficient for a decisive judgment. This judgment is node-level visual evidence computed for each relevant entity and does not convert a mere entity mention into an explicit existence evidence unit. The regeneration model directly uses this precomputed judgment rather than inferring entity existence again from $p_{\text{yes}}(o)$.

For 2D relative relations, the report provides a precomputed *Layout judgment*; for absolute image positions, it provides a *Frame judgment*; and for relative-depth relations, it provides a precomputed *Depth judgment*. A geometric judgment is treated as decisive only when all involved entities are reliably determined to be present and are assigned to the HIGH tier. If an absolute-position or relation evidence unit is contradicted because an involved entity is reliably determined to be absent, the report explicitly identifies the violation of its entity-existence presupposition. If entity existence is uncertain or geometric reliability is insufficient, the evidence unit is reported as INCONCLUSIVE. The reasoning model directly uses these precomputed judgments rather than reinterpreting raw bounding boxes, grounding scores, or depth values.

Let the set of evidence units contradicted by reliable visual evidence be

$$\mathcal{S}^- = \{s_m \mid \text{ver}(s_m) = \text{CONTRADICTED}\}.$$

If this set is nonempty, we select the earliest contradicted evidence unit according to the provenance index k_m stored in the SEG:

$$s^\star = \arg\min_{s_m \in \mathcal{S}^-} k_m.$$

If multiple contradicted evidence units share the earliest source-step index, the first unit according to their original order within that reasoning step is selected.

The earliest contradicted evidence unit $s^\star$ is highlighted in the verification report, while relevant SUPPORTED and INCONCLUSIVE judgments are also retained. SUPPORTED results help the model preserve already correct judgments, whereas INCONCLUSIVE results indicate that the available evidence is insufficient and should not be treated as mandatory correction signals.

C.3 Targeted Reasoning Regeneration

When a reliable contradiction is found, the original image, original question, initial reasoning chain, initial answer, verification report, and dataset-specific answer-format requirements are jointly provided to the same MLLM that generated the initial reasoning. The model is not required to reinterpret the low-level visual evidence; instead, it revises the localized error according to the verified spatial judgments in the report.

During regeneration, the model is instructed to preserve judgments consistent with reliable evidence, revise the earliest contradicted evidence unit $s^\star$, and regenerate the affected reasoning from its source step together with the final answer. If a spatial-relation evidence unit is contradicted because an involved entity is reliably determined to be absent, the model should remove or revise the unsupported relation rather than infer the opposite spatial relation.

The model is not required to repeat existence probabilities, reliability scores, bounding boxes, grounding scores, depth values, or other low-level evidence in its output. Evidence units marked as INCONCLUSIVE must not be treated as decisive correction signals.

When no reliable contradiction is identified, i.e., $\mathcal{S}^- = \varnothing$, regeneration is not performed, and the initial reasoning chain and answer are retained. This fallback strategy prevents unnecessary modifications caused by MEDIUM- or LOW-reliability evidence or uncertain existence evidence.

The entire correction process is performed using the original MLLM and requires no task-specific model fine-tuning or parameter updates.

C.4 Reasoning Regeneration Prompt

The complete prompt used for targeted reasoning regeneration is shown in Tab. 10. Its placeholders are replaced with the original question, initial reasoning, initial answer, generated verification report, and answer-format requirements of the corresponding dataset.

D Answer Evaluation Prompts

Evaluation protocol. For RealWorldQA, GQA, and POPE, we first apply deterministic answer-

extraction and normalization rules. GPT-4o is invoked as a text-only semantic evaluator only when the rule-based procedure is inconclusive. For all GPT-4o evaluations, we set the temperature to 0 and the maximum number of output tokens to 8, and use the same system prompt. For RealWorldQA, GQA, and POPE, only the last 4,500 characters of the model response are retained for evaluation.

GPT-4o-based binary semantic accuracy. For LLaVA-Bench-in-the-Wild and MMHal-Bench, we do not use exact string matching. Instead, all valid samples are evaluated using GPT-4o-based binary semantic judgments. The evaluator returns YES when the response correctly answers the question and is semantically consistent with the reference answer, and NO otherwise. Synonyms, paraphrases, and harmless formatting or detail differences are accepted, whereas materially incorrect answers, contradictions, failures to answer, or unsupported statements that change the answer's meaning are judged incorrect.

A YES judgment is recorded as `correct=true`, whereas a NO judgment is recorded as `correct=false`. The reported accuracy is the proportion of successfully scored samples judged as YES:

$$\mathrm{Acc}_{\text{GPT-4o}} = \frac{N_{\text{correct}}}{N_{\text{scored}}},$$

where N_{correct} is the number of samples judged as YES, and N_{scored} is the number of samples for which a valid binary judgment is successfully obtained. Samples that cannot be scored successfully are excluded from the denominator.

E Self-Revision Prompt

Tab. 15 presents the complete prompt used for the generic Self-Revision baseline.

Prompt used for targeted reasoning regeneration
You are given an image, a question, your previous reasoning and final answer, and a verification report containing spatial judgments derived from reliable visual evidence. Question: {Original question} Previous reasoning: {Previous reasoning} Previous final answer: {Previous final answer} Verification Report: {Verification Report, i.e., additional_information} Report interpretation rules: - Follow the precomputed Existence judgment for each entity: PRESENT indicates reliable presence, ABSENT indicates reliable absence, and UNCERTAIN indicates insufficient existence evidence. - Do not infer that every entity mentioned in the report is present in the image. - Use the precomputed Layout judgment to determine left/right/above/below relations. - Use the precomputed Frame judgment to determine an object's absolute position in the image. - Use the precomputed Depth judgment to determine closer/farther or front/behind relations. - Do not reinterpret or recompute a judgment from the reported probability, reliability score, bounding box, grounding score, or depth value. - A SUPPORTED result should be preserved unless it is affected by the correction of an earlier contradicted evidence unit. - A CONTRADICTED result should be revised according to the corresponding precomputed visual judgment. - If a relation is CONTRADICTED because an involved entity is ABSENT, remove or revise the unsupported relation; do not infer the opposite spatial relation. - An INCONCLUSIVE result is not a mandatory correction signal. Do not force a spatial judgment from inconclusive evidence. - Do not replace a 2D left/right relation with a depth or front/behind relation, or vice versa. Correction instructions: - Revise the highlighted earliest contradicted evidence unit and regenerate the affected reasoning from its source step together with the final answer. - Preserve earlier reasoning steps and other judgments that remain consistent with the verified evidence. - Ensure that the regenerated reasoning and final answer are mutually consistent. - Do not introduce unsupported objects, attributes, or spatial relations. - Do not repeat the verification evidence, probabilities, reliability scores, bounding boxes, grounding scores, or depth values in your reasoning. - Think step by step. Preserve the original step-based reasoning format whenever possible, and return the revised reasoning followed by the final answer. {Dataset-specific answer-format requirements}

Table 10: Prompt used to guide targeted reasoning regeneration using the verification report.

Common system prompt used for answer evaluation
Reply with exactly YES or NO. No punctuation or explanation.

Table 11: Common system prompt used for GPT-4o-based answer evaluation.

Prompt used for evaluating LLaVA-Bench-in-the-Wild and MMHal-Bench
You are a strict correctness grader for {benchmark_name}. Evaluate the model response as a binary correct/incorrect visual-question-answering response. Return YES when it correctly answers the question and is semantically consistent with the reference answer. Synonyms, paraphrases, and harmless formatting or detail differences are acceptable. The reference answer is not necessarily the only valid wording. Return NO for a materially wrong answer, contradiction, failure to answer, or unsupported statements that change the answer's meaning. A clear factual contradiction anywhere in the response makes it incorrect. Question: {question} Reference answer: {gt} Model response: {model_answer} Reply with exactly one token: YES if correct, otherwise NO.

Table 12: Binary semantic-correctness prompt used for LLaVA-Bench-in-the-Wild and MMHal-Bench. The placeholder {benchmark_name} is replaced with the corresponding benchmark name.

Prompt used for evaluating RealWorldQA and GQA
You are a strict grader for vision-language QA. Decide whether the model's answer expresses the SAME final choice as the ground truth. - For multiple-choice, same option letter (or same wording as the labeled choice) counts as match. - For two-option word questions (e.g. two nouns), treat synonyms or clear paraphrases as match only if they pick the same entity. - Ignore harmless formatting differences. Question (may be empty): {question} Ground truth (GT): {gt} Model response (may include long chain-of-thought; judge the intended final answer): {model_answer} Reply with exactly one token: YES if equivalent, otherwise NO.

Table 13: Semantic-equivalence prompt used for RealWorldQA and GQA when deterministic answer extraction and normalization are inconclusive.

Prompt used for evaluating POPE
You are a strict grader for vision-language QA. Decide whether the model's answer expresses the SAME final choice as the ground truth. - For multiple-choice, same option letter (or same wording as the labeled choice) counts as match. - For two-option word questions (e.g. two nouns), treat synonyms or clear paraphrases as match only if they pick the same entity. - Ignore harmless formatting differences. This is a POPE-style binary task: ground truth is exactly YES or NO (object existence in the image). Decide whether the model's intended final judgment matches that YES/NO, even if the model did not print the word "yes" or "no" clearly. Question (may be empty): {question} Ground truth (GT): {gt} Model response (may include long chain-of-thought; judge the intended final answer): {model_answer} Reply with exactly one token: YES if equivalent, otherwise NO.

Table 14: Binary object-existence evaluation prompt used for POPE when deterministic answer extraction is inconclusive.

Prompt used for Self-Revision
You are given an image, a question, and your previous reasoning and final answer. Please carefully reconsider the previous reasoning based on the image and the question. Check whether each step is consistent with the visual content and whether the final answer follows from the reasoning. Do not assume that the previous reasoning or answer is incorrect. Preserve correct judgments and revise only the parts that you independently determine should be changed. Question: {question} Previous reasoning: {previous_cot} Previous final answer: {previous_answer} Please provide your revised reasoning and final answer in the following format: Reasoning: <your revised reasoning> Final Answer: <your final answer>

Table 15: Complete prompt used for the generic Self-Revision baseline.